Supplementary Information

Ternary blend organic solar cells with improved morphological stability

Minwoo Nam,‡[a] Jaehong Yoo,‡[a] Yunjae Park,‡[b] Hye Yeon Noh,[a] Yongkook Park,[a] Junhee Cho,[a] Jung-A Kim,[a] Jehan Kim,[c] Hyun Hwi Lee,[c] Rakwoo Chang*[b] and Doo-Hyun Ko*[a]

[a]Department of Applied Chemistry, Kyung Hee University, Yongin, Gyeonggi 17104, Republic of Korea

[b]Department of Chemistry, Kwangwoon University, Seoul 01897, Republic of Korea

[c]Pohang Accelerator Laboratory, Pohang, Gyeongbuk 37673, Republic of Korea

Supplementary Method

Details for the MD analysis of the OSC system are as follows. First, each donor/acceptor molecule was divided into several simple fragments. For instance, the PTB7-Th monomer unit was fragmented into 8 small fragments (named BNDT, FDTP, 2 THIP, ACE, and 3 2EHP moieties) (Fig. S15). $PC_{70}BM$ and ITIC-Th molecules were also divided into 2 and 11 fragments, respectively (Fig. S16). Next, the force field parameters (including atomic charge, bond, angle, and dihedral potential parameters) were obtained using the CGenFF program.[1] In the case of the FDTP fragment, the atomic charges were not well supported by the CGenFF program; thus, the geometry was optimized using MP2/6-31G(d), and the atomic charges were obtained using the Merz-Singh-Kollman method.[2] The resulting atomic charges of the FDTP fragment are given in Fig. S17. Since the conformations of complex molecules are mainly affected by the dihedral angle potentials between fragments, we additionally optimized several major dihedral potentials using the lsfitpar program (Fig. S18).[3]

The PTB7-Th molecule was modelled as a connected chain of 8 PTB7-Th monomer units in this simulation study. A total of 17 PTB7-Th molecules were randomly inserted into a simulation box $10 \times 10 \times 20$ nm^3 in dimensions. This monomer concentration, which was about 10 times as high as the experimental condition, was used to accelerate the solvent evaporation process. Both $PC_{70}BM$ and ITIC-Th molecules were then randomly inserted into the simulation box based on the experimental donor:acceptor weight ratios. For instance, there were 172 $PC_{70}BM$ for PTB7-Th:$PC_{70}BM$, 124 ITIC-Th for PTB7-Th:ITIC-Th, and 105 $PC_{70}BM$ and 52 ITIC-Th for PTB7-Th:$PC_{70}BM$:ITIC-Th systems. Finally, chlorobenzene molecules were added into the void space as solvents. The resulting solvent molecules added in each system were about 9400 for PTB7-Th:$PC_{70}BM$, 9000 for PTB7-Th:ITIC-Th, and

9200 for PTB7-Th:$PC_{70}BM$:ITIC-Th systems.

MD simulations for the three OSC systems were performed using the NAMD MD software package (version 2.9).[4] The simulation temperature was set to 333.15 K (60 °C) using the Nose-Hoover thermostat.[5] To mimic the solvent evaporation process, the box lengths in both x and y directions were fixed to 10 nm, but a constant pressure of 1 atm was applied to the z direction using the Nose-Hoover Langevin piston barostat.[6]

Lee and Pao's scheme was employed to mimic the solvent evaporation process.[7] First, each system was equilibrated before the solvent evaporation process was initiated. Then, 10% of the solvent molecules were removed from the system. Since the solvent removed system was unstable, a short energy minimization of 1000 steps was run. The resulting system was again equilibrated for 5 ns. After 5 ns, the same number of solvent molecules was again removed from the system. This solvent-removal process was repeated until no solvent molecules were left in the system (total 45 ns). The solvent evaporation rate in this simulation was much faster than the experimental condition, which usually takes several hours at least, but it still provides significant insights into the qualitative behaviour of the OSC morphology change for different composition conditions. Representative snapshots of both initial and final (solvent 0%) configurations in each system are shown in Figs. 5a-c. It is also noted that independent initial configurations for each system were used to provide better statistics for the simulation results of the solvent evaporation process.

Table S1 Photovoltaic parameters of ternary OSCs with different ITIC-Th concentrations under AM 1.5G 1 sun illumination. The average and standard deviation values were obtained from more than 10 cells for each kind of device.

ITIC-Th concentration	V_{OC} (V)	J_{SC} (mAcm^{-2})	FF (%)	PCE (%)
ITIC-Th 0%	0.76	14.29 (± 0.24)	48.18 (± 0.35)	5.22 (± 0.15)
ITIC-Th 20%	0.80	19.34 (± 0.25)	55.99 (± 0.96)	8.70 (± 0.25)
ITIC-Th 40%	0.81	19.62 (± 0.16)	56.99 (± 0.58)	8.91 (± 0.10)
ITIC-Th 60%	0.80	18.35 (± 0.13)	58.37 (± 1.21)	8.66 (± 0.25)
ITIC-Th 80%	0.79	18.12 (± 0.11)	60.85 (± 0.70)	8.71 (± 0.12)
ITIC-Th 100%	0.78	17.21 (± 0.12)	63.17 (± 0.92)	8.44 (± 0.17)

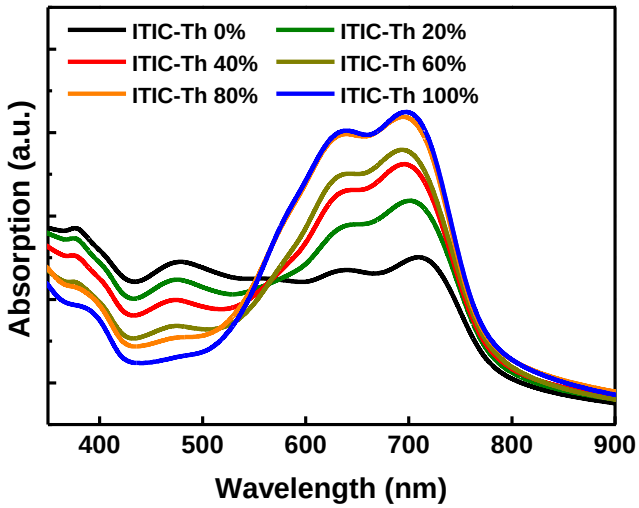

Fig. S1 UV-vis absorption spectra of PTB7-Th:$PC_{70}BM$:ITIC-Th ternary BHJ films for different ITIC-Th concentrations ($PC_{70}BM$:ITIC-Th = 100:0, 80:20, 60:40, 40:60, 20:80, or 0:100).

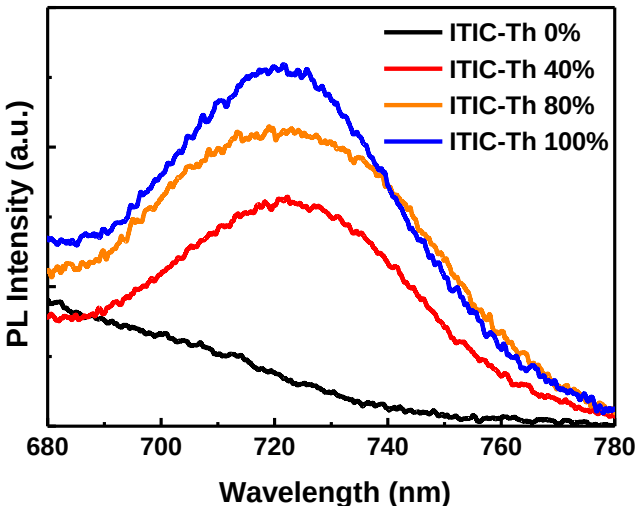

Fig. S2 Steady-state PL spectra of neat $PC_{70}BM$, neat ITIC-Th, and $PC_{70}BM$:ITIC-Th films. The excitation wavelength of 468 nm is within the main absorption regime of $PC_{70}BM$, and thus was selected to check whether the energy transfer occurs from $PC_{70}BM$ to ITIC-Th. The PL quenching of ITIC-Th when mixed with $PC_{70}BM$ indicates the likelihood of charge transfer (rather than energy transfer) process at $PC_{70}BM$:ITIC-Th junctions. Considering the *J*–*V* results of the acceptor-only devices in Figure 1d, we could confirm the charge transfer mechanism between $PC_{70}BM$ and ITIC-Th in our ternary system.

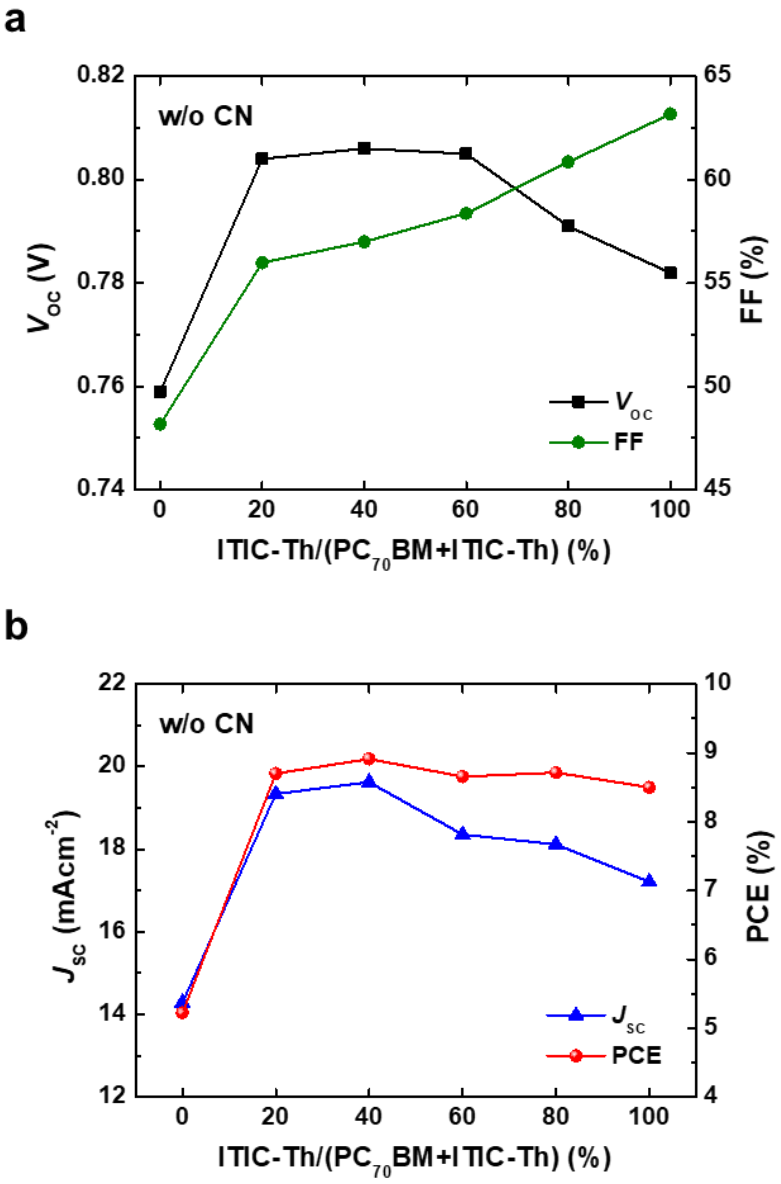

Fig. S3 Photovoltaic parameters of the ternary OSCs with varying $PC_{70}BM$:ITIC-Th ratios in the absence of CN solvent additive: a) V_{OC} and FF and b) J_{SC} and PCE. The mean values obtained from more than 10 devices are provided.

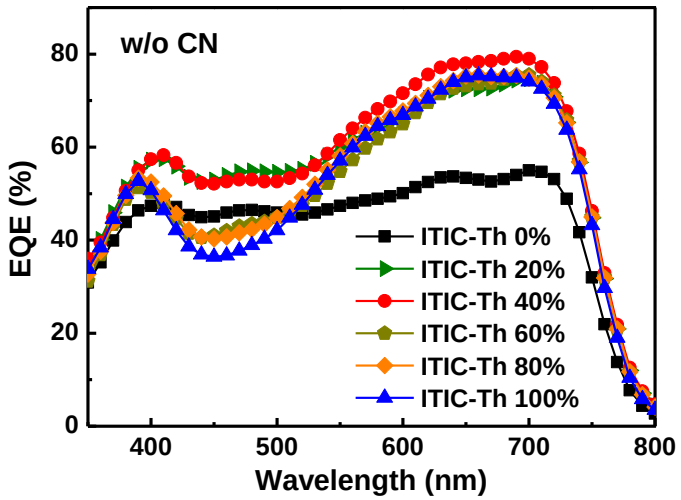

Fig. S4 EQE spectra of ternary OSCs with varying ITIC-Th concentrations.

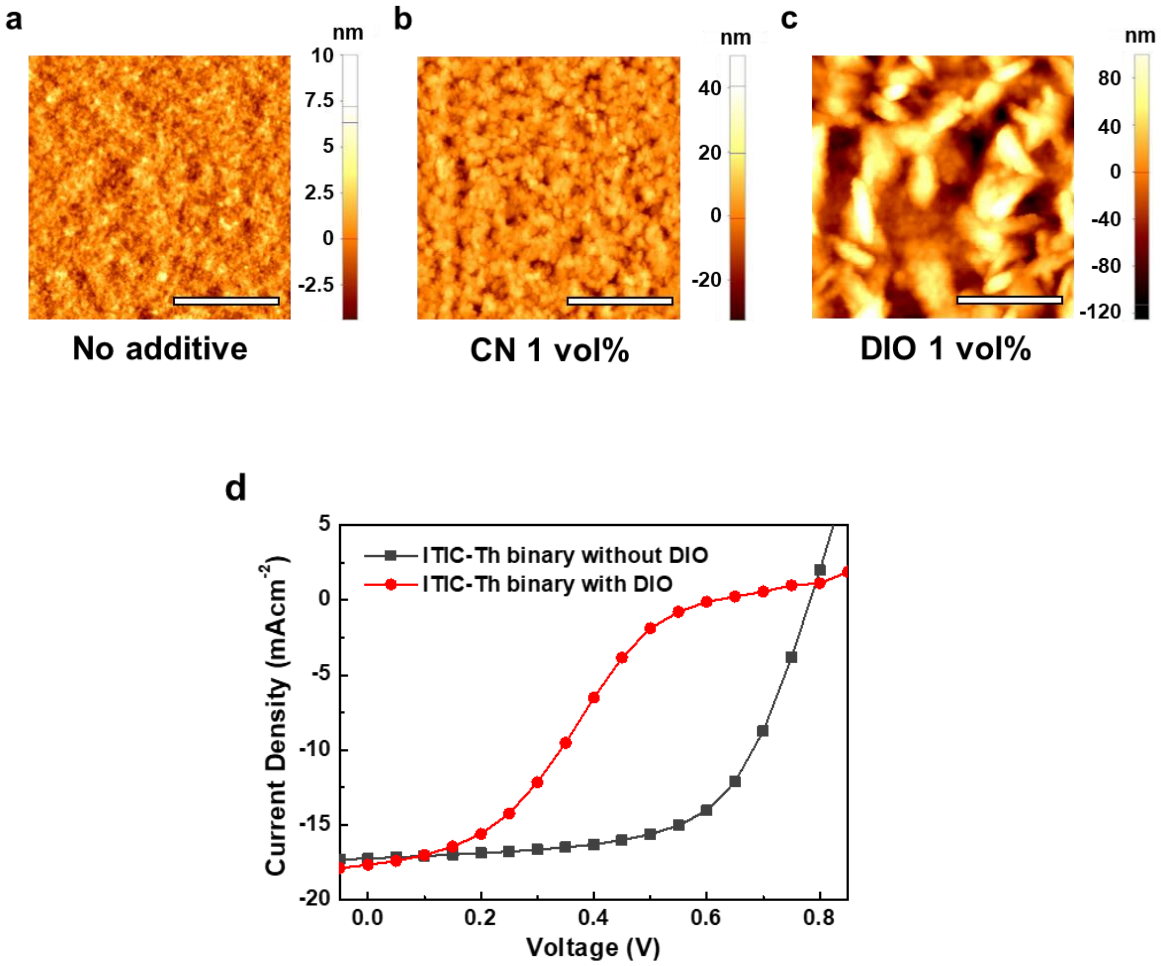

Fig. S5 AFM height images of ITIC-Th binary blends (a) without additive, (b) with 1 vol% CN, and (c) with 1 vol% DIO. The scale bars indicate 2μm. (d) *J*-*V* characteristics of ITIC-Th binary OSCs without or with DIO.

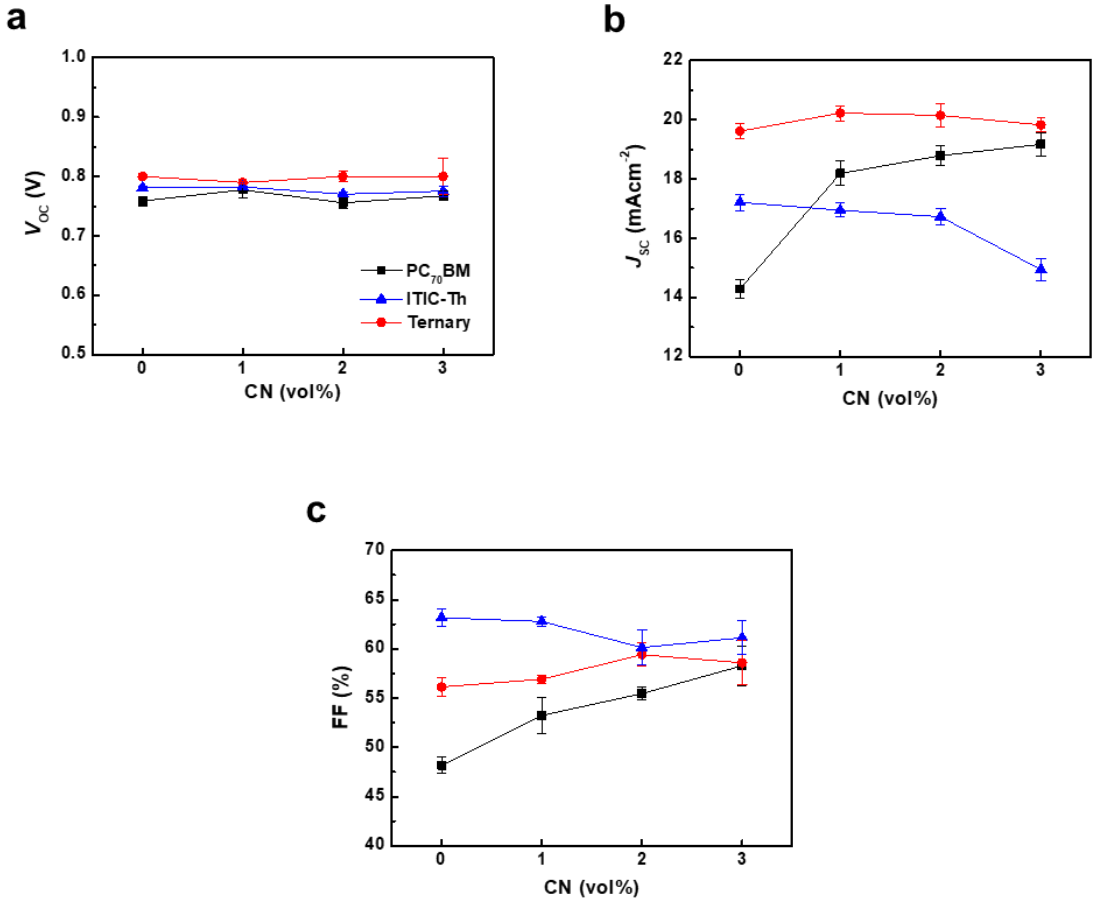

Fig. S6 Photovoltaic parameters of three devices for different CN concentrations: a) V_{OC}, b) J_{SC}, and c) FF. The average and standard deviation values were obtained from more than 10 devices.

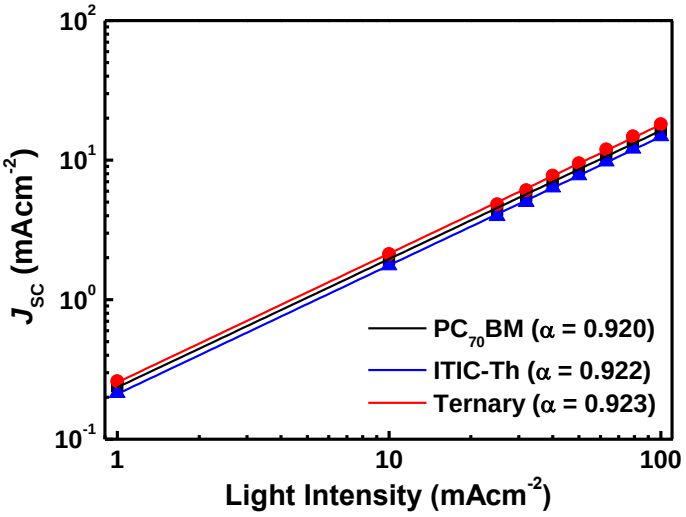

Fig. S7 Dependence of J_{SC} on the incident light intensity (P_{in}) for three devices showing a similar slope (α) of 0.92.

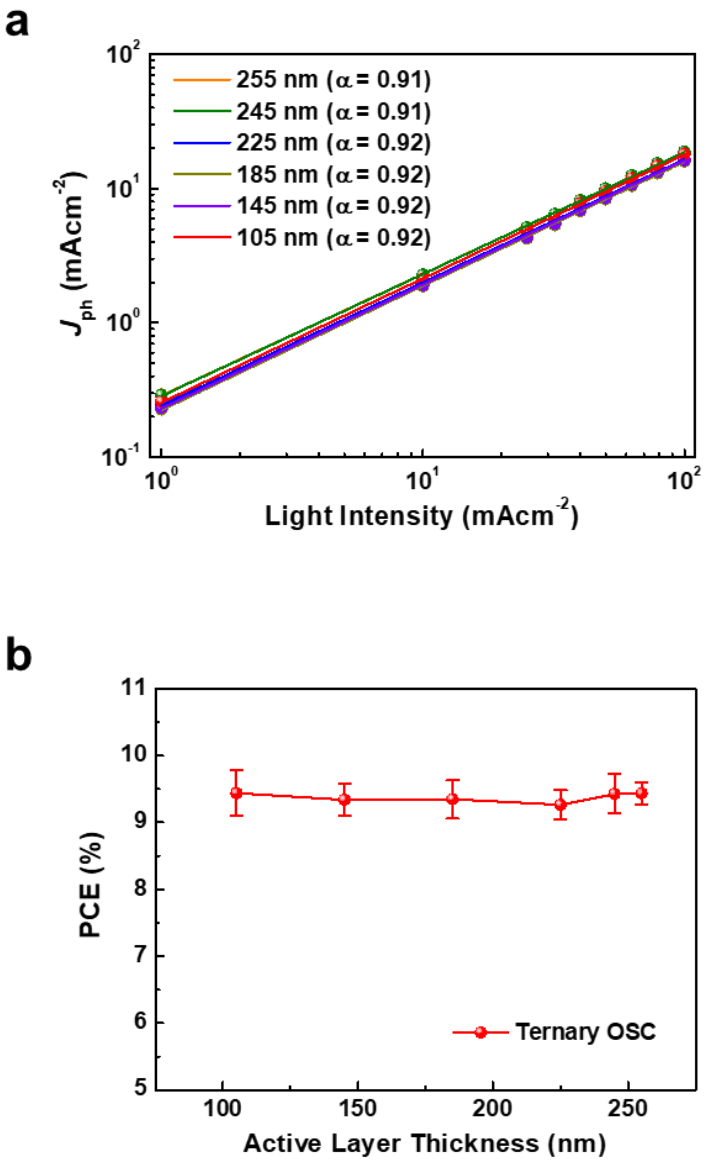

Fig. S8 (a) P_{in}-J_{ph} characteristics and (b) PCE of ternary OSCs as a function of active layer thickness. The mean values were obtained from more than 10 cells and error ranges correspond to respective standard deviation values.

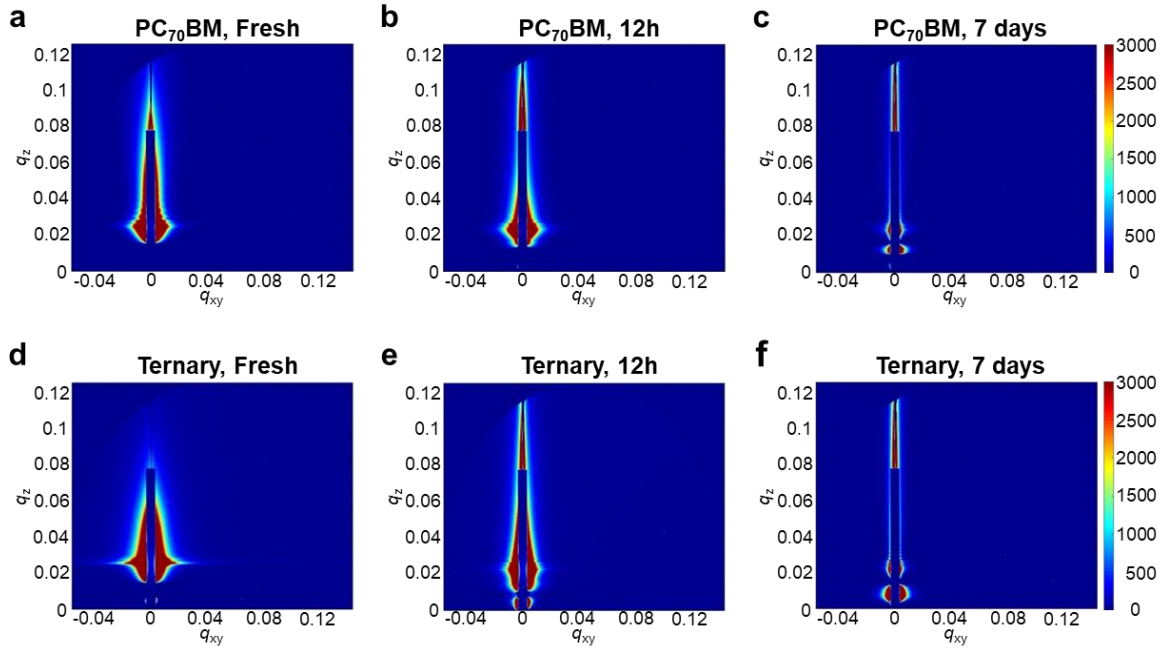

Fig. S9 GISAXS patterns of blends with different annealing durations at 60 °C: (a-c) $PC_{70}BM$ binary and (d-f) ternary blends.

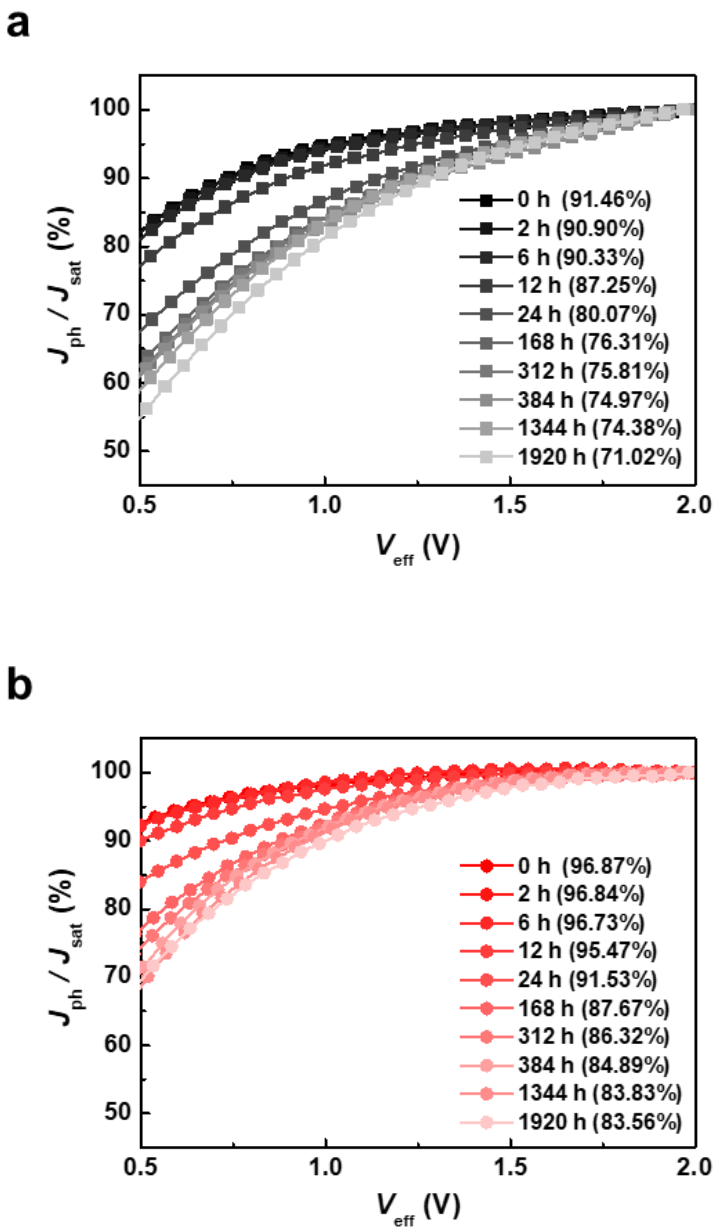

Fig. S10 Charge transfer analysis. J_{ph}/J_{sat} properties of (a) $PC_{70}BM$ binary and (b) ternary OSCs as a function of V_{eff}. The percentage values in the legends indicate *P(E,T)* values under short conditions.

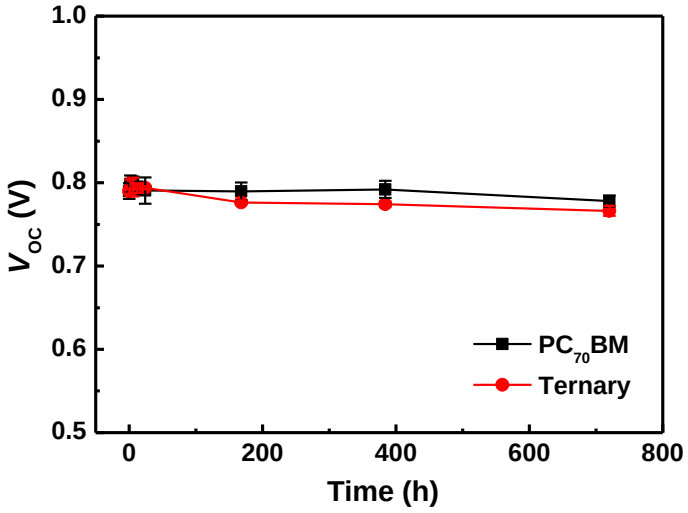

Fig. S11 Long-term stability. Time-dependent V_{OC} of $PC_{70}BM$ binary and ternary OSCs under thermal treatment at 60 °C. The mean values with standard deviation were obtained from more than 8 devices.

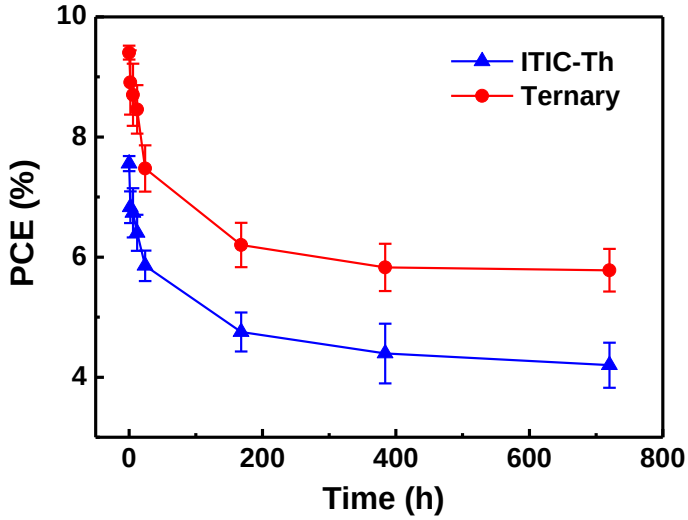

Fig. S12 PCE variation of ITIC-Th binary OSC relative to the ternary OSC as a function of thermal treatment time at 60 °C.

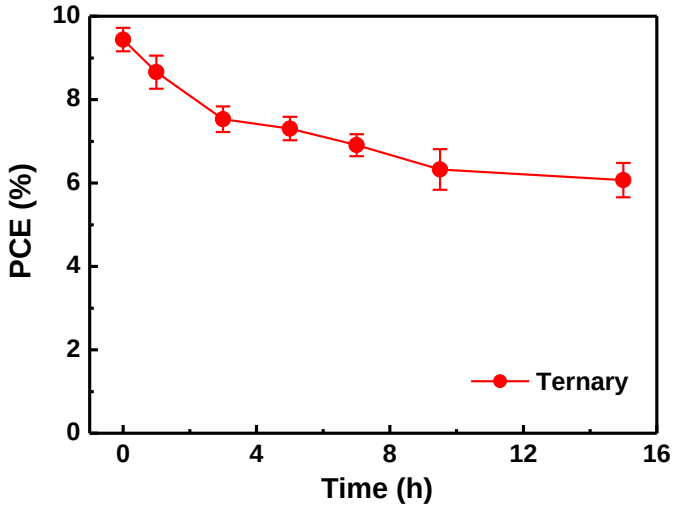

Fig. S13 Photo-induced PCE decay of the ternary OSC under continuous AM 1.5G illumination (100 mWcm^{-2}).

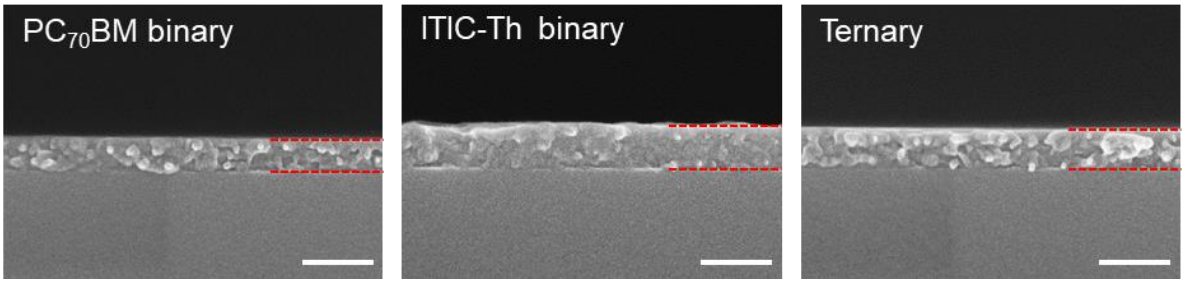

Fig. S14 Cross-sectional SEM images of active layers with different compositions. The active layer is defined with red dashed lines, and the scale bars denote 200 nm.

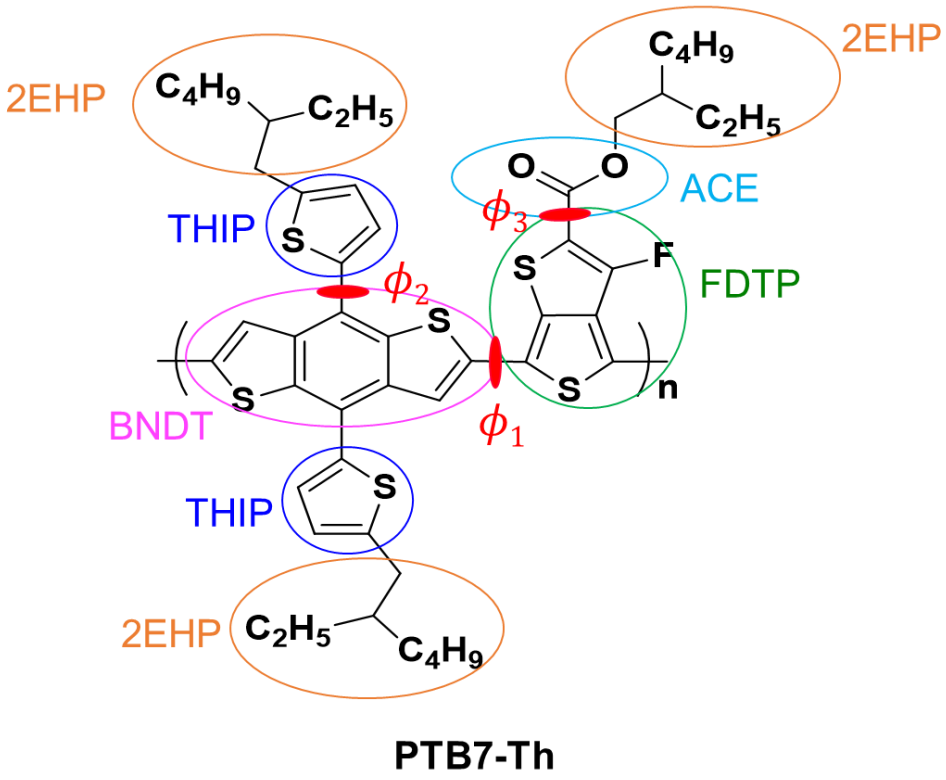

Fig. S15 Force field parameterization scheme of PTB7-Th. The PTB7-Th monomer unit was divided into 8 small fragments (named BNDT, FDTP, 2 THIP, ACE, and 3 2EHP moieties). The dihedral angle potentials around the bonds marked with red ellipses (ϕ_1~ϕ_3) were additionally parameterized using the lsfitpar program (see Fig. S18).

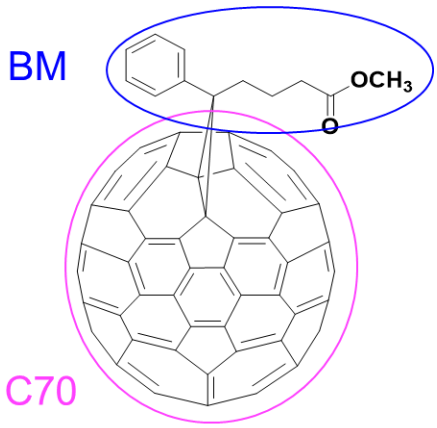

$PC_{70}BM$

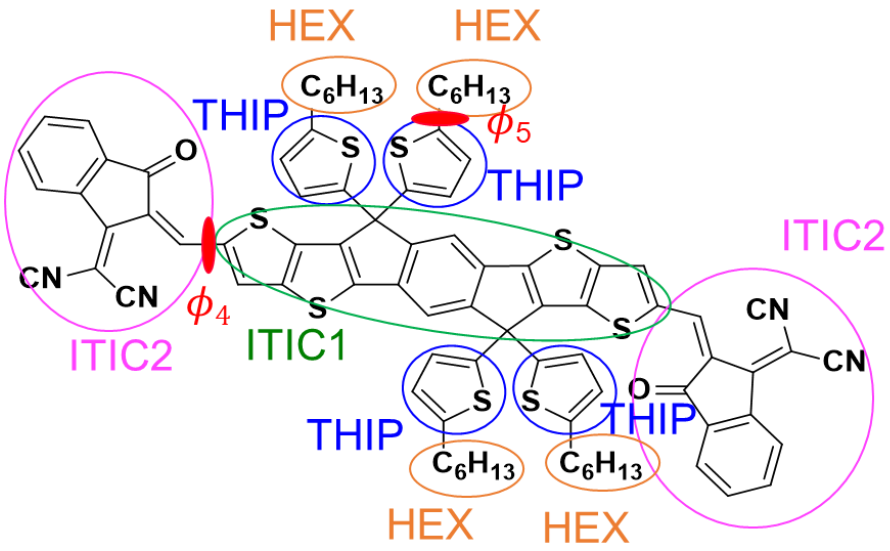

ITIC-Th

Fig. S16 Force field parameterization schemes of $PC_{70}BM$ and ITIC-Th. The dihedral angle potentials around the bonds marked with red ellipses ($\phi_4 \sim \phi_5$) were additionally parameterized using the lsfitpar program (see Fig. S18).

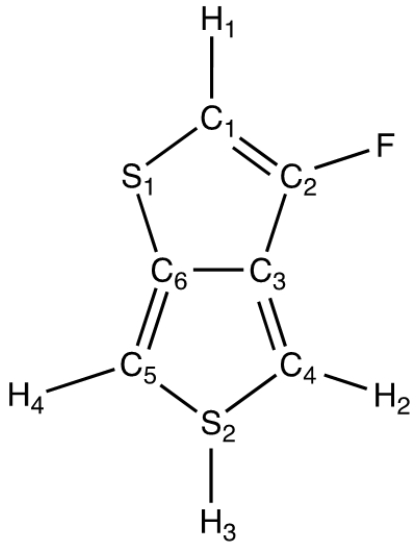

Atom	Charge (e)
S1	0.002
C1	-0.397
H1	0.268
C2	0.244
F	-0.168
C3	0.112
C4	-0.319
H2	0.233
S2	0.077
C5	-0.278
H3	0.245
C6	-0.019

Fig. S17 Structure and atomic charges of the FDTP moiety. The geometry was optimized using MP2/6-31G(d) and the atomic charges were obtained using the Merz-Singh-Kollman method.

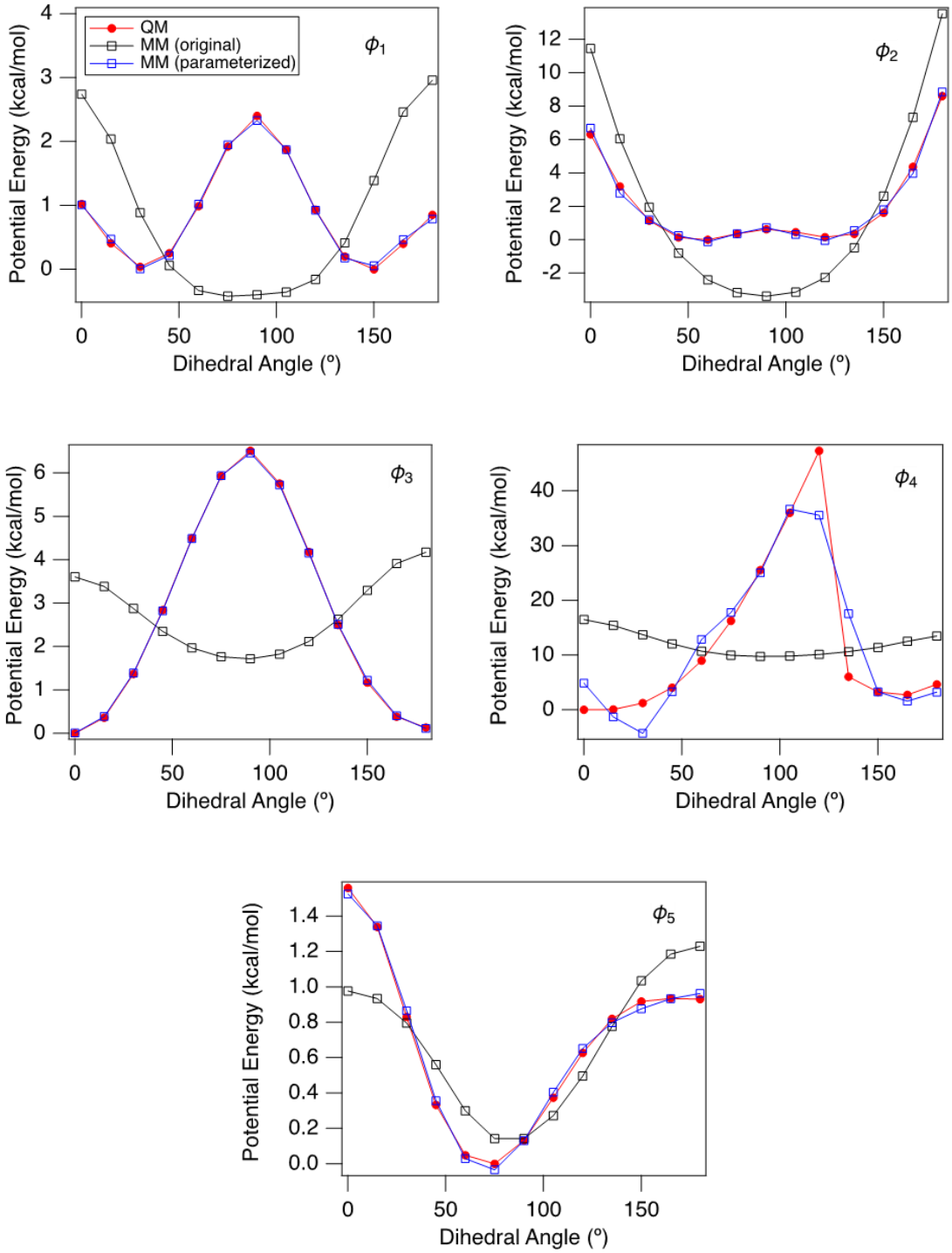

Fig. S18 Dihedral angle potential parametrization (ϕ_1~ϕ_5). Red, black, and blue lines correspond to quantum calculation, original, and parameterized CHARMM General Force Fields, respectively.

Supplementary References

1. cgenff.paramchem.org
2. U. C. Singh and P. A. Kollman, *J. Comput. Chem.,* 1984, **5**, 129.
3. K. Vanommeslaeghe, M. Yang and A. D. MacKerell Jr., *J. Comput. Chem.,* 2015, **36**, 1083.
4. L. Kalé, R. Skeel, M. Bhandarkar, R. Brunner, A. Gursoy, N. Krawetz, J. Phillips, A. Shinozaki, K. Varadarajan and K. Schulten, *J. Comput. Phys.,* 1999, **151**, 283.
5. D. J. Evans and B. L. Holian, *J. Chem. Phys.,* 1985, **83**, 4069.
6. S. E. Feller, Y. Zhang, R. W. Pastor and B. R. Brooks, *J. Chem. Phys.,* 1995, **103**, 4613.
7. C.-K. Lee and C.-W. Pao, *J. Phys. Chem. C,* 2014, **118**, 11224.